Supporting Information

A near-infrared-II light-response BODIPY-based conjugated microporous polymer for enhanced photocatalytic degradation of cationic dyes and H_2O_2 production

Xiaobo Luo[a,1], Yan Zhang[a,1], Shiyuan Zhou[a,*], Peng Wang[b,*], Danfeng Wang[a,c], Peiyang Gu[a,*]

Affiliations:

[a]*Engineering Laboratory of Functional Nano- and Microstructured Materials in Petroleum and Chemical Industry, School of Petrochemical Engineering, Changzhou University, Changzhou, 213164, PR China. E-mail address: gupeiyang0714@cczu.edu.cn (P. Gu) & zhoushiyuan@cczu.edu.cn (S. Zhou)*

[b]*College of Biological, Chemical Science and Chemical Engineering, Jiaxing University, Jiaxing 314001, China. pengwang@zjxu.edu.cn (P. Wang),*

[c]*State Key Laboratory of Treatments and Recycling for Organic Effluents by Adsorption in Petroleum and Chemical Industry, Soochow University, Suzhou, 215123, China*

[1]*These authors contributed equally to this work.*

Contents

1. Methods and synthetic procedure

Materials and methods

Methanol, Ethanol, dichloromethane, triethylamine (TEA), K_2CO_3, N,N-dimethylformide (DMF), diisopropylamine (DiPA), and THF were obtained from Sinopharm Reagent Co., Ltd. and were of analytical grade and used without further purification. triphenylphosphine (PPh_3), CuI, methylene blue (MB), methylene orange (MO) Rhodamine B (RhB),were purchased from Energy Chemical. β-carotene, and Nafion were obtained from Aladdin. 2,4-dimethyl-1H-pyrrole, N-iodosuccinimide (NIS), 1 M tetrabutylammonium fluoride in tetrahydrofuran, 5,5-dimethyl-1-pyrroline, benzoyl chloride, N-oxide (DMPO), resorcinol, p-hydroxybenzaldehyde and 2,2,6,6-Ttetramethyl-piperidinyloxy 1-oxyl (Tempo) were purchased from TCI (Tokyo Chemical Industry). Bis(triphenylphosphine) palladium (II) chloride ($Pd(PPh_3)_2Cl_2$), tetra(triphenylphosphine)palladium ($Pd(PPh_3)_4$) and trimethylsilane acetylene (TMSA) were provided by Sigma-Aldrich.

Characterization

A Fourier transform infrared (FT-IR) spectrophotometer (Thermo Scientific Co., United States, Nicolet 6700) was used to measure the FT-IR spectra of samples using KBr pellet. The solid-state ^{13}C NMR was measured on a Bruker INOVA 400 MHz NMR spectrometer. The N_2 adsorption-desorption isotherms were performed on a Quantachorme Micromeritics ASAP 2020 instrument at 77 K. Based on the N_2 adsorption-desorption data, the Brunauer-Emmett-Teller (BET) method was used to calculate the specific surface area of the samples. The powder X-ray diffraction (PXRD) of the samples was performed on an X'Pert-Pro MPD analyzer. The surface morphology of TPEs is observed by scanning electron microscope (SEM, Merlin Compact, Japan) and transmission electron microscopy (TEM, FEI-Tecnai G2 F20, USA). The hydrophilicity and hydrophobicity of TPEs are measured in a water contact angle analyzer. The thermal stability of the materials is tested by thermogravimetric analysis (TGA, TG209F3, Germany) from 30 ℃ to 700 ℃ with the heating rate of 10 ℃ min^{-1}. The surface chemistry of the catalysts is analyzed by a X-ray photoelectron

spectroscopy (XPS, ESCALAB 250, USA).The absorption of POPs at solid state was measured by a UV-Vis spectrophotometer (Shimadzu, UV3600). The residual concentration of organic dyes were analyzed by UV-vis. Electrochemical properties were studied by an electrochemical workstation (CHI760E, Shanghai, China).The signals of active radicals were detected by an electron spin resonance (ESR) spectrometer (JEOL, JES-X320).

2. Synthetic procedure

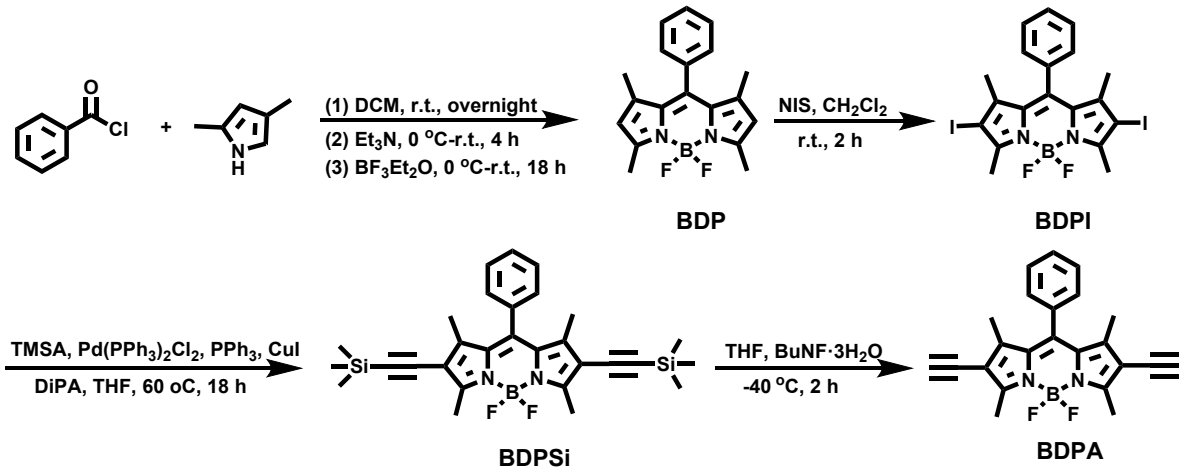

Scheme S1. The synthetic procedure towards BDP, BDPI, BDPSi, and BDPA.

Synthesis of **BDP**: **BDP** was synthesized according to the literature with modifications[1]. Under a nitrogen atmosphere, benzoyl chloride (2.8 g, 2.3 mL, 20 mmol) and 2,4-dimethylpyrrole (3.7 g, 4.0 mL, 40 mmol) were added to dry CH_2Cl_2 (150 mL) using a syringe. The mixture was stirred at room temperature overnight. The Et_3N (20 mL) was added under the ice-cold condition and reacted for 4 h. The mixture was then cooled to 0 °C, $BF_3{\cdot}Et_2O$ (20 mL) was added, and then the mixture was warmed to room temperature and stirred overnight. Next, the mixture was poured into water (200 mL), and the organic layer was concentrated under reduced pressure. The crude product was purified by column chromatography (silica gel, CH_2Cl_2: n-hexane = 1 : 2, v/v) to afford the title compound as a dark green powder. Yield: 2.0 g, 6.16 mmol, 31 %. ^{1}H NMR (300 MHz, $CDCl_3$), δ 7.49–7.47 (m, 3H, Ar-H), 7.29–7.26 (m, 2H, Ar-H), 5.98 (s, 2H, Pyrrole-H), 2.56 (s, 6H, Pyrrole-CH_3), 1.37 (s, 6H, Pyrrole-CH_3). The data is in good accordance to the literature report

BDPI was synthesized according to a literature procedure with modifications.[1] **BDP** (4.0 g, 12.4 mmol) was dissolved in dry CH_2Cl_2 (100 mL), then *N*-iodosuccinimide (NIS, 6.7 g, 30 mmol) was added into the solution of **BDP** slowly under the ice-cold condition. After the addition, the mixture was stirred at room temperature for 5 h. The solvent was removed under reduced pressure and the crude product was purified by column chromatography on silica gel (CH_2Cl_2 : *n*-hexane = 1: 2, v/v). Yield: 6.0 g, 10.41 mmol, 84 %. ^{1}H NMR (300 MHz, $CDCl_3$) δ 7.52 (m, 3H, Ar-H), 7.25 (m, 2H, Ar-H), 2.64 (s, 6H, pyrrole-CH_3), 1.38 (s, 6H, pyrrole-CH_3). The data is in good accordance to the literature report.

Synthesis of **BDPSi**: Under a nitrogen atmosphere, **BDPI** (6.8 g, 11.8 mmol), $Pd(PPh_3)_4Cl_2$ (874.8 mg, 1.2 mol), PPh_3 (547.0 mg, 2.2 mmol) and CuI (711.0 mg, 7.9 mmol) were mixed in diisopropylamine (100 mL) and tetrahydrofuran (THF, 200 mL). After stirring, trimethylsitylacetylene (TMSA, 10.0 g, 20 mL, 101.8 mmol) was added using a syringe. The solution was stirred at 60 ^{o}C for 4 h. After the completion of the reaction ,the solvent was removed under reduced pressure and the crude product was purified by column chromatography on silica gel (CH_2Cl_2) to obtain a dark-red solid. Yield: 5.2 g, 10.06 mmol, 85 %. ^{1}H NMR (300 MHz, $CDCl_3$): 0.29 (s, 18H, Si-CH_3), 1.36 (s, 6H, pyrrole-CH_3), 2.53 (s, 6H, pyrrole-CH_3), 7.12-7.32 (m, 5H, Ar-H). The data is in good accordance to the literature report [2].

Synthesis of **BDPA**: Under a nitrogen atmosphere, tetrabutylammonium fluoride (TABF, 1M in THF, 80 mL) was added dropwise to a solution of **BDPI** (4.9 g, 9.4 mmol) in 100 mL THF at -40 ^{o}C and the solution was kept at -40 ^{o}C for 4 h. After the completion of the reaction, CH_2Cl_2 (100 mL) and H_2O (100 mL) were added. The organic layer was separated and concentrated under reduced pressure to give out the crude product. Then, the crude product was purified by column chromatography on silica gel (*n*-hexane:CH_2Cl_2 = 5:1, v/v) to give the product as a red powder. Yield: 3.0 g, 8.05 mmol, 85 %[2]. ^{1}H NMR (300 MHz, $CDCl_3$): 1.37 (s, 6H, pyrrole-CH_3), 2.53 (s, 6H, pyrrole-CH_3), 3.36 (s, 2H), 7.12-7.30 (m, 5H, Ar-H).

Synthesis of Calixarene: Resorcinol (2.22 g, 20.17 mmol) was dispersed in 60 mL ethanol in a 250 mL Schlenk flask under a N_2 atmosphere with ice bath. 10 mL of

concentrated hydrochloric acid was added into the above solution slowly. Then, 4-hydroxybenzaldehyde (2.44 g, 19.99 mmol, dissolved in 10 mL of ethanol) was slowly added to the reaction system. Once the reaction solution returned to room temperature, it was heated and refluxed for 12 h. Afterwards, the mixture was washed and recrystallized by ethanol to obtain 3.5 g pink product with a yield of 81%[3] ^{1}H NMR (400 MHz, DMSO-d_6) δ 8.84 (s, 4H), 8.44 (s, 8H), 6.64 (d, J = 8.3 Hz, 9H), 6.52 – 6.42 (m, 11H), 6.08 (s, 4H), 5.52 (s, 4H) (**Fig. S1**).

Synthesis of LBFD-1: In a 500 mL Schlenk flask, 2,8-diethynyl-5,5-difluoro-1,3,7,9-tetramethyl-10-phenyl-5H-4l4,5l4-dipyrrolo[1,2-c:2',1'-f][1,3,2]diazaborinine (BDPA, 1.78 g, 4.8 mmol) and 1,3,5-trifluoro-2,4,6-triiodobenzene (1.63 g, 3.2 mmol) were dissolved in a mixed solvent of N, N-dimethylformide (DMF) and diisopropylamine (DiPA) (250 mL, v/v = 3:2) followed by the addition of CuI (54.7 mg, 0.288 mmol) and $Pd(PPh_3)_4$ (222 mg, 0.19 mmol) under a N_2 atmosphere. The reaction solution was heated to reflux for 3 d. The precipitate was filtered and Soxhlet extracted with THF, CH_3OH, and CH_2Cl_2, respectively. After being dried at 60 ℃ under vacuum overnight, 1.29 g of black powder was obtained.

Synthesis of LBFD-2: LBFD-1 (0.69 g) was dispersed in 30 mL DMF in a 100 mL Schlenk flask under a N_2 atmosphere, then calixarene (1.28 g, 1.5 mmol) and anhydrous K_2CO_3 (2.76 g, 20 mmol) were added to the reaction solution. The mixture was heated to reflux for 3 d. Afterwards, the mixture solution was filtered and washed with methanol, then dried at 60 ℃ under vacuum to obtain 1.04 g of black product.

3. Experiments

Photodegradation Experiments

The photocatalytic degradation of pollutants was tested under simulated sunlight (a 300 W Xe lamp). Before the experiment, 8 mg of LBFD-2 was homogeneously dispersed in 16 mL of organic pollutants solutions (MB 200 ppm and RhB 50 ppm). The solutions were firstly stirred in the dark and 1 mL of suspension was taken every 5 min. After 15 min, the solution was irradiated with an Xe lamp with circulating water to prevent solvent evaporation caused by overheating. 1 mL of suspension was taken

every 5 min for UV-Vis analysis through a 0.22 μm filter syringe.

Photocatalytic H_2O_2 production experiments

5 mg of photocatalyst was added to 20 mL of distilled water and exposed to air in a custom flask. A 300 W Xe lamp (300-2500 nm, 1200 mW/cm^2) was used for illumination. After certain time intervals, the H_2O_2 production was measured by potassium titanium oxalate method described in the following section.

Detection method of H_2O_2

The H_2O_2 concentration in the heterogeneous solution was determined by a potassium titanium oxalate method. Firstly, the potassium titanium oxalate solution (0.02 M) was prepared by dissolving anhydrous $C_4H_2K_2O_{10}Ti$ (1.77 g) in H_2SO_4 aqueous solution (12 mL 98% H_2SO_4 + 50 mL deionized water), then deionized water was added until the total volume reached 250 mL. Secondly, after given time intervals, 1.5 mL of suspension was filtrated with a 0.22 μm filter followed by the addition of 1 mL of potassium titanium oxalate solution (0.02 M). The concentration of H_2O_2 was calculated based on the change of absorbance at 400 nm by a UV–vis spectrophotometer[4].

Calibrations for the measurements of H_2O_2 solution

Low concentration curves:

3 mL of H_2O_2 solutions with the concentrations of 0.1, 0.2, 0.4, 0.6, 0.8, 1 mmol/L were prepared. 2 mL of potassium titanium oxalate solution was used as the color indicator and the mixture solution was shaken and then kept still for 3 min. UV-vis spectra of the solution were recorded by using a UV vis spectrophotometer at 400 nm. The linear relationship between H_2O_2 concentration and the absorption intensity was shown in the following picture:

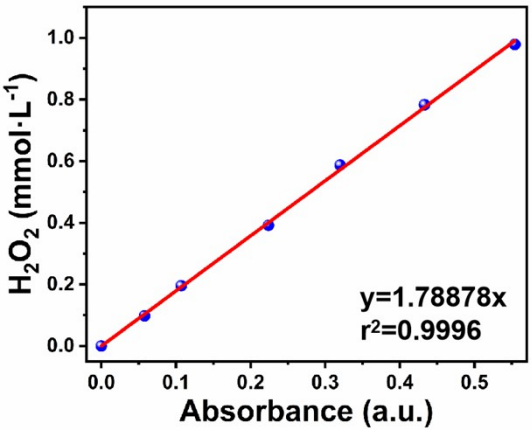

High concentration curves:

1 mL of H_2O_2 solutions with the concentrations of 1, 2, 4, 6, 8, 10 mmol/L were prepared. 9 mL of potassium titanium oxalate solution was used as the color indicator and the mixture solution was shaken and then kept still for 3 min. The linear relationship between H_2O_2 concentration and the absorption intensity was shown in the following picture:

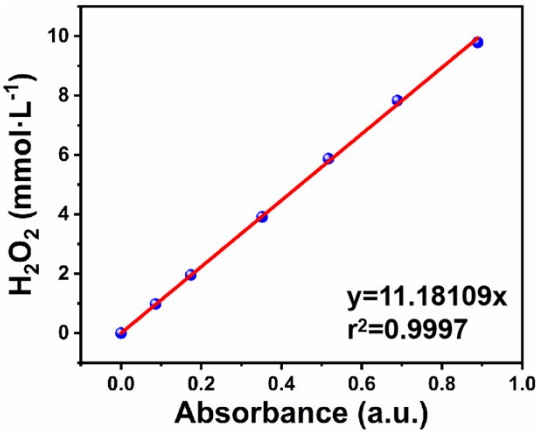

Cyclic experiments

Before the experiment, 40 mg LBFD-2 were uniformly dispersed in 80 mL MB (200 ppm) and RhB (50 ppm) solution, and the photodegradation experiment in a single cycle was the same with the above procedure. Afterwards, the photocatalyst was centrifuged and washed with ethanol three times by filtration, then dried for the next cycle.

Radical trapping experiments

8 mg of LBFD-2 was dispersed in 16 mL of organic pollutants solutions (MB 200 ppm and RhB 50 ppm) and quantitative free radical capture agents were added after adsorption in the dark for 15 min. Then the solution was irradiated with a 300 W Xe lamp and the following procedure was the same with the above photocatalytic degradation experiments.

Photoelectrochemical measurements

The method for preparing the working electrodes was as follows: Add 5 mg of catalyst to 2 mL of ethanol, then add 20 μL of 5 wt% Nafion dispersed in the above solution by ultrasound. Next, drop the solution onto the surface of ITO (1 cm×2 cm) glass and vacuum dry for 30 minutes. Use a 0.5 M Na_2SO_4 solution as the electrolyte, and Ag/AgCl electrode and platinum wire as the reference electrode and counter electrode, respectively.

ESR experiments

10 mg of catalyst were dispersed in 5 mL pure water and sonicated for 15 min. For the detection of •OH, DMPO was used and prepared in 100 mM aqueous solution, and for the detection of $^1O_2$, TEMP was used and prepared in 100 mM aqueous solution. In a 5 mL brown glass vial, 200 μL of the catalyst suspension and 200 μL of DMPO/TEMP solution were mixed and sonicated for 5 min. The resulting suspension was then placed into a capillary and subjected to ESR instrument for scanning 50 s under both dark condition and light condition.

4. Equations

$$Eg = E_{VB} - E_{CB} \quad \text{(S1)}$$

5. Results and discussion

Fig. S2a showed that the peak in the range of 1500-1600 cm^{-1} was corresponding to the stretching vibration of the aromatic skeleton and the peaks at 3200 and 2200 cm^{-1} were attributed to the stretching vibration of -OH and -C≡C- groups, respectively, which proved the successful synthesis of LBFD-1. Moreover, a new peak at 1100 cm^{-1} belonging to -C-O-C- group appeared, indicating the successful introduction of calixarene moiety to produce LBFD-2. Meanwhile, as shown in **Fig. S2b**, for LBFD-1,

the peaks in the range of δ=7-25 ppm was attributed to the methyl group in BODIPY and the peaks at δ=112, 129, 140 ppm were assigned to the alkyne carbons, the aromatic carbons and the aromatic C-F bonds, respectively. For LBFD-2, the peaks in the range of δ=30-45 ppm and the peak at δ=153 ppm were attributed to the methylene carbons and the carbons linked to phenolic groups, respectively, which were derived from the addition of calixarene moiety. Moreover, the intensity of the peak at δ=140 ppm belonging to the carbons in the C-F bonds decreased, demonstrating the success of the nucleophilic substitution reaction and the incorporation of calixarene moiety. Additionally, as shown in **Fig. S3-4**, the XPS spectra of LBFD-1 and LBFD-2 exhibited the peaks attributed to the C, N, O, F and B elements. For LBFD-1, in the high-resolution XPS spectra of C 1s, B 1s and N 1s, the peaks at 288.7, 287.5, 286.0, 284.4 and 284.0 eV were attributed to the C-F, C-N, C=N, C-C and C≡C bonds; the peaks at 192.0 and 187.0 eV were assigned to the B-N and B-F bonds; the peaks at 400.0, 399.2 and 398.5 eV were belonging to the B-N, C-N and C=N bonds, respectively. Moreover, For LBFD-2, the addition of calixarene moiety resulted in several changes in the high resolution XPS spectra. For example, a new peak corresponding to the C-O bonds appeared at 285.5 eV in that of C 1s and two new peaks attributed to C-O bonds and -OH groups at 532.7 and 531.8 eV emerged, further proving the successful introduction of calixarene moiety. Therefore, the above characterizations indicated that the structures of LBFD-1 and LBFD-2 had been successfully constructed.

Additionally, the Brunauer-Emmett-Teller (BET) surface areas of LBFD-1 and LBFD-2 were measured by the N_2 adsorption-desorption curves (**Fig. S2c-d**) to be 18.8 and 6.5 $m^2 g^{-1}$, respectively, and the pore size distribution indicated that the pore width of LBFD-1 and LBFD-2 were mainly located at 1.88 and 1.82 nm, respectively, which demonstrated the microporous nature of these CMPs-based photocatalysts. The thermal stability of LBFD-1 and LBFD-2 were investigated by the thermogravimetric analysis (TGA). As shown in **Fig. S5**, when reaching 5% weight loss, the temperatures of LBFD-1 and LBFD-2 were 294 and 182 °C, respectively, indicating their excellent thermal stability.

Fig. S10 showed the influence of photocatalyst dosage on the removal

performance towards MB. The increasing dosages of photocatalyst contributed to the degradation performance of MB. However, the adsorption rate of LBFD-2 with dosage of 1 mg mL^{-1} in dark was too fast, thus it is difficult to carry out further investigation including different pH, water sources, competing ions, *etc*. Although the adsorption rate in dark with dosage of 0.5 mg mL^{-1} was poorer than that of 1 mg mL^{-1}, it can still reach η>99% within 20 min, thus the dosage of 0.5 mg mL^{-1} was chosen as the optimal dosage.

As displayed in **Fig. S11**, the pH primarily affected the adsorption process in the dark. When at pH=3, the LBFD-2 was positively charged, while when pH＞5, it became negatively charged (**Fig. S12**), and the absolute value increased with the increasing pH, contributing to the electrostatic interaction with MB and as a result, improving the removal performance under alkaline conditions. However, for RhB, the removal performance of LBFD-2 was inhibited under alkaline conditions, which was mainly attributed to the formation of RhB dimers and consequently, increasing the difficulty of RhB entering the porous skeleton of LBFD-2. Moreover, the influence of different real-water sources including Yangtze river, lake and tap waters on the photocatalytic degradation towards MB and RhB was crucial owing to the existence of various inorganic substances and microorganisms, which were the excellent candidates for the simulation of real water treatment scenarios. The three kinds of water sources all exhibited inhibition effect on the removal performance, and among them, the tap water showed the strongest inhibition effect probably owing to the residue of Cl^- in it during the disinfection process, which was confirmed by the further investigation on the influence of competing ions. Various aqueous solutions of competing anions including Cl^-, NO_2^-, $H_2PO_4^{2-}$ and SO_4^{2-} (20 mM) were prepared to simulate the inorganic ions in real-water scenarios. Among them, the Cl^- exhibited obvious inhibition effect on the removal performance of LBFD-2 towards both MB and RhB since the Cl^- contributed to the aggregation of dye molecules, forming dimers and increasing the molecular volume, consequently enhancing the difficulty for them to enter the pores of the catalyst[5], and the result was consistent with that of the real-water sources experiment. However, the addition of $H_2PO_4^{2-}$ significantly improved the removal performance

because due to the reverse Hofmeister effects, the $H_2PO_4^{2-}$ was a salt-in anion and could increase the solubility of dye molecules, facilitate the passage of dye molecules through the pores, thereby enhancing the adsorption efficiency[6]. On the contrary, the addition of NO_2^- and SO_4^{2-} had little influence on the adsorption and degradation processes.

The control experiment in darkness for comparison had been performed and shown in **Fig. S17**. The anionic dyes were desorbed by washing with methanol after both the adsorption process in dark and degradation process under visible light irradiation. 70% of RhB and 66% of MB can be desorbed after the adsorption process in dark, while only 26% of RhB and 7% of MB were desorbed after the photodegradation process in light. This phenomenon indicates that the photodegradation primarily contributed to the removal performance of LBFD-2 and the majority of RhB and MB had been degraded into diverse intermediates.

With respect to the degradation pathways of RhB, two main pathways were proposed (**Fig. S21**)[7, 8]. Firstly, RhB was attacked by ROS, leading to demethylation and the formation of intermediate 1 (m/z=415), which was further transformed into intermediate 2 (m/z=387). In pathway I, the benzoic acid moiety was decomposed to form intermediate 3 (m/z=283) and 4 (m/z=269); in pathway II, the amino and quaternary ammonium groups were gradually decomposed to form intermediate 5 (m/z=316) and 6 (m/z=302). Through oxidation and ring-opening reactions, various small molecular intermediates including 7 (m/z=166), 8 (m/z=122) and 9 (m/z=148) were generated from the intermediates 4 and 6. Moreover, these intermediates underwent ring-opening reactions to form intermediates 10 (m/z=90), 11 (m/z=102), and 12 (m/z=132), which were mineralized to CO_2 and H_2O, consequently completing the degradation process.

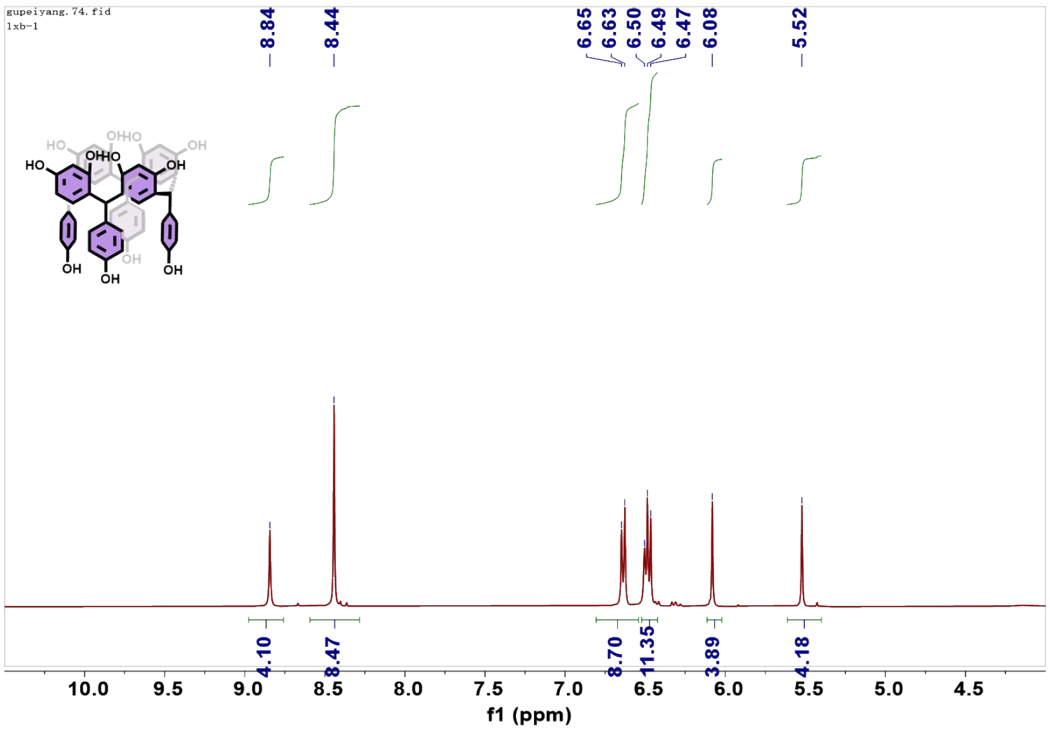

Fig. S1 The ^{1}H NMR spectrum of Resorcinarene (DMSO-d_6).

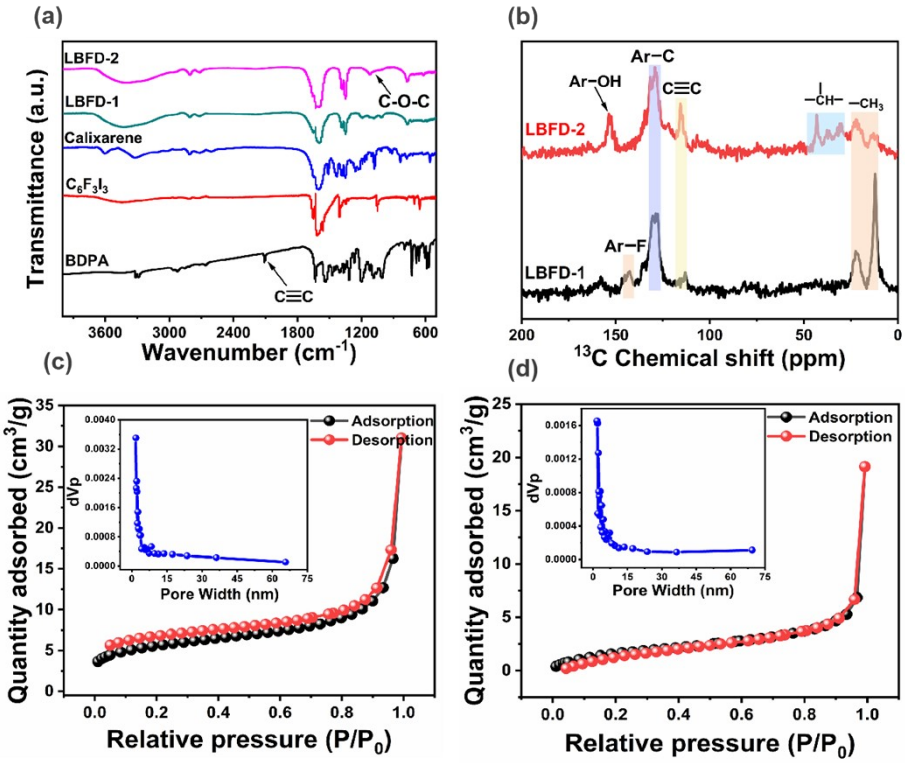

Fig. S2 The (a) FT-IR and (b) ss-^{13}C NMR spectra of LBFD-1 and LBFD-2; the BET curves of (c) LBFD-1 and (d) LBFD-2. Inset: the corresponding pore size distributions.

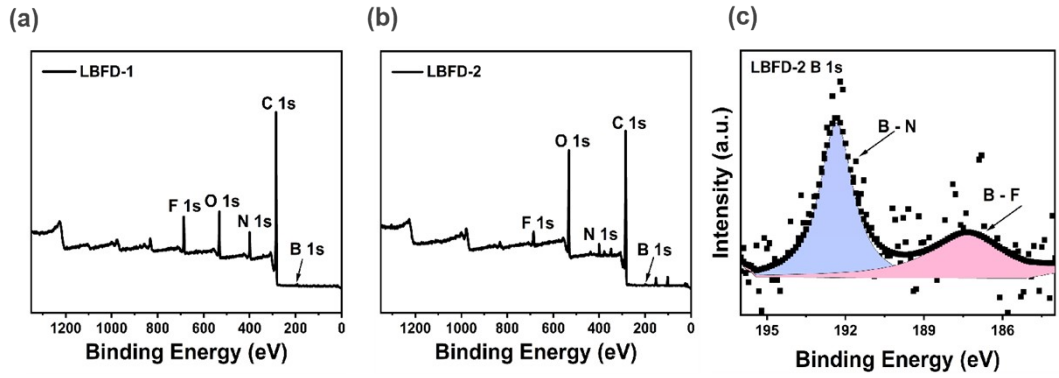

Fig. S3 The XPS spectra of (a) LBFD-1 and (b) LBFD-2; (c) the high-resolution XPS spectra of B 1s in LBFD-2.

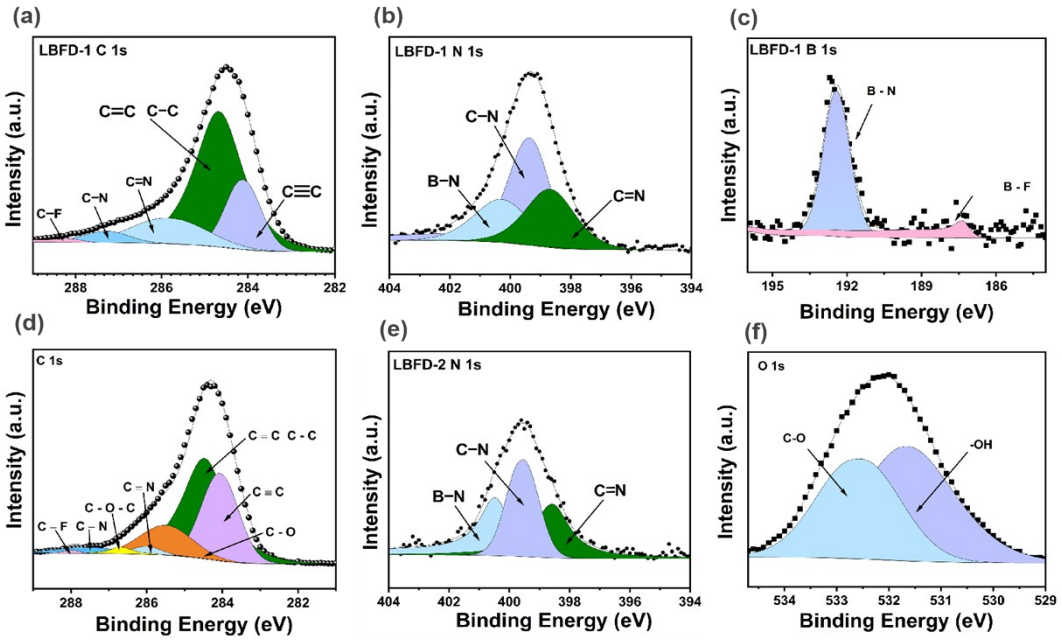

Fig. S4 The high-resolution XPS spectra of (a) C 1s, (b) N 1s, (c) B 1s in LBFD-1 and (d) C 1s, (e) N 1s, (f) O 1s in LBFD-2.

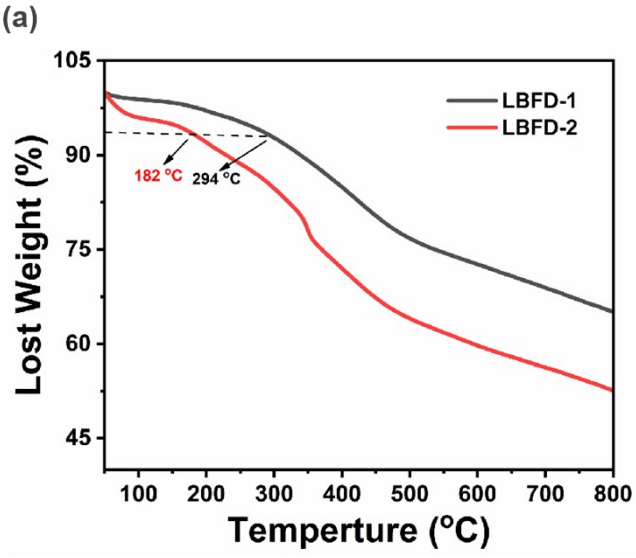

Fig. S5 The TGA curves of LBFD-1 and LBFD-2.

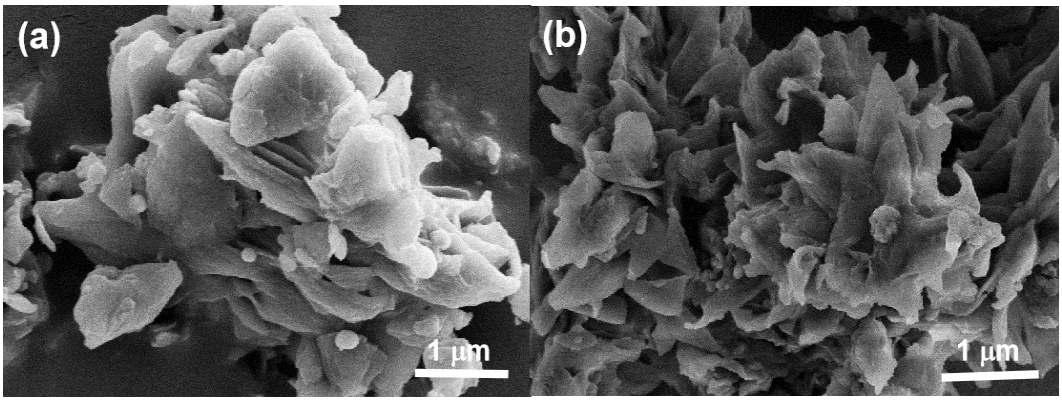

Fig. S6 The SEM images of (a) LBFD-1, (b) LBFD-2.

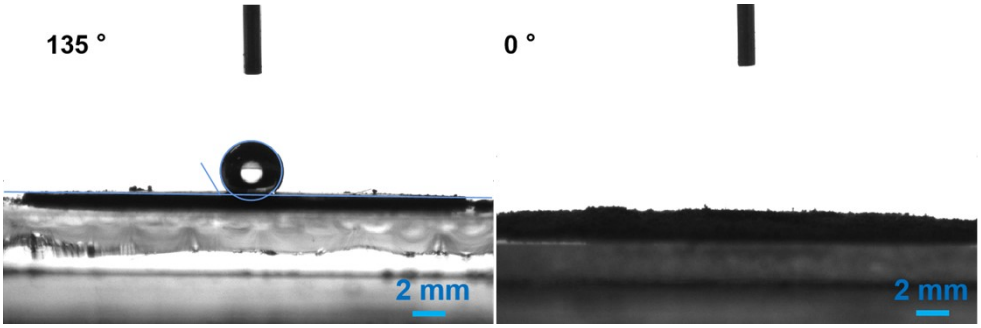

Fig. S7 The water contact angles of (a) LBFD-1 and (b) LBFD-2.

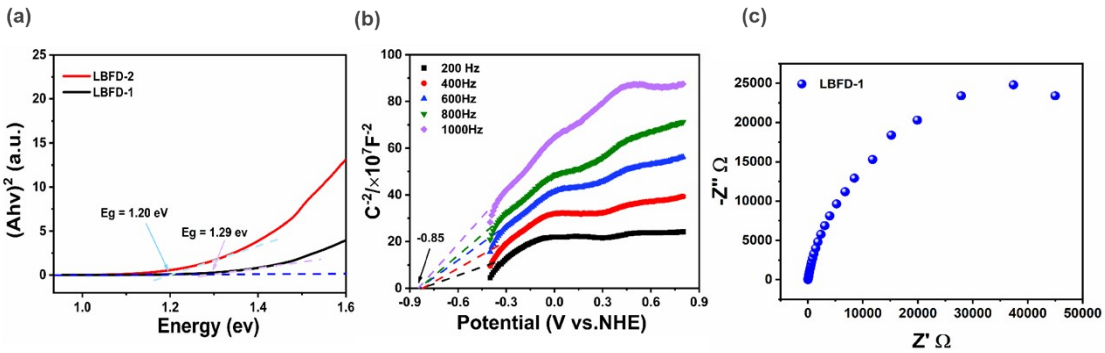

Fig. S8 (a) The Tauc plots of LBFD-1 and LBFD-2; the (b) Mott-Schottky plots and (c) electrochemical impedance of LBFD-1.

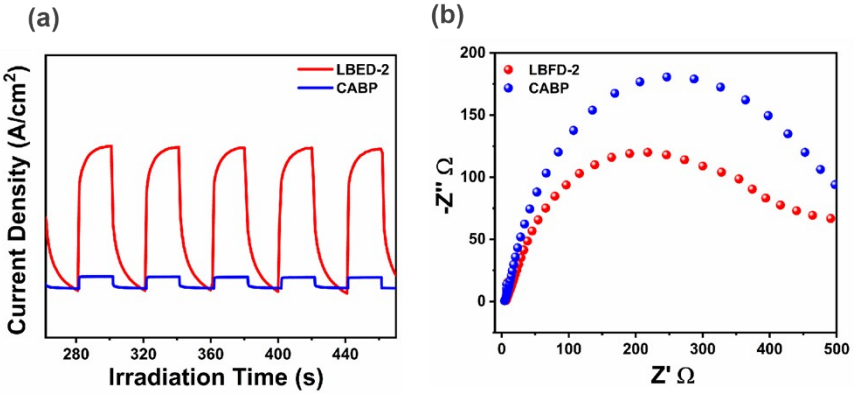

Fig. S9 (a) The photocurrent curves and (b) electrochemical impedance of CABP and LBFD-2.

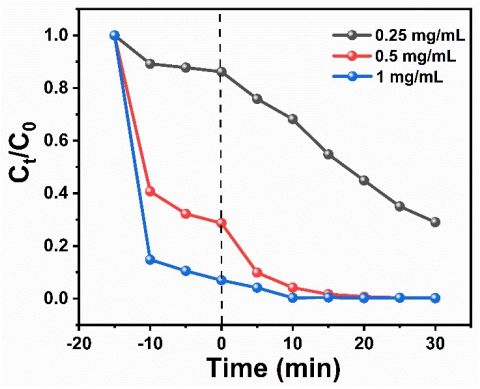

Fig. S10 The photodegradation performance of LBFD-2 towards MB with different dosages of photocatalyst. Concentration of MB: 200 ppm.

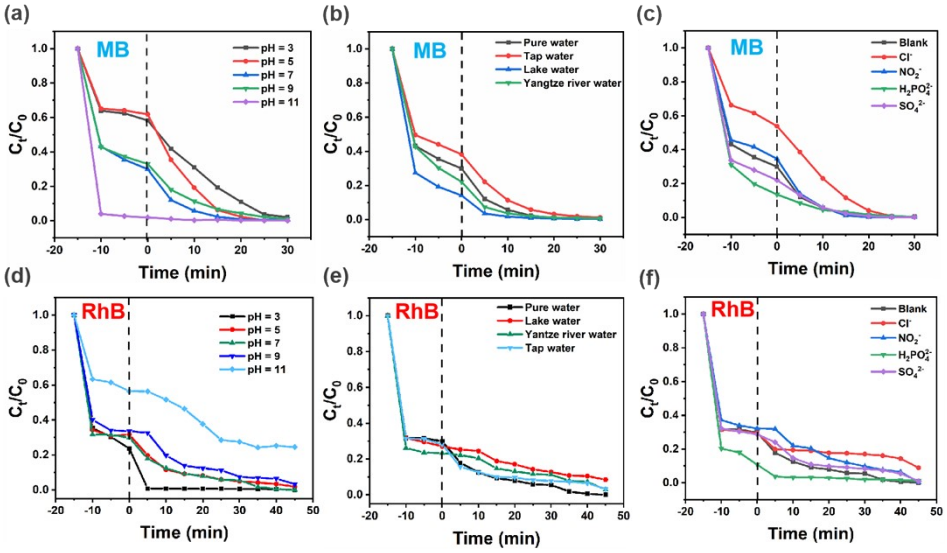

Fig. S11 The influence of different factors including pH, environmental waters and competing anions on the photodegradation performance of LBFD-2 towards (a-c) MB and (d-f) RhB. Concentration of MB: 200 ppm. Concentration of RhB: 50 ppm. Dosage of catalysts: 0.5 mg mL^{-1}.

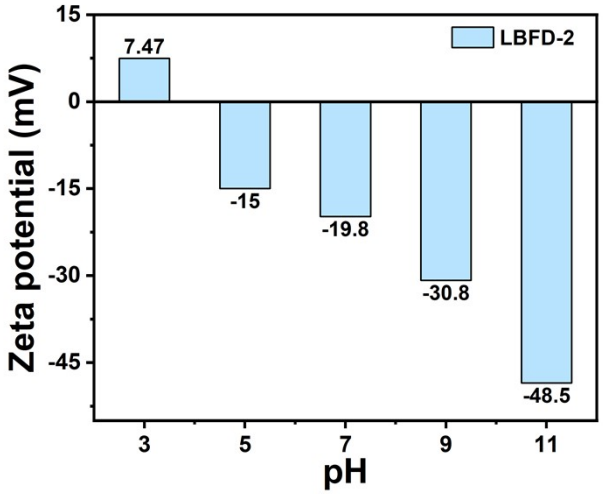

Fig. S12 The zeta potential of LBFD-2 at different pH.

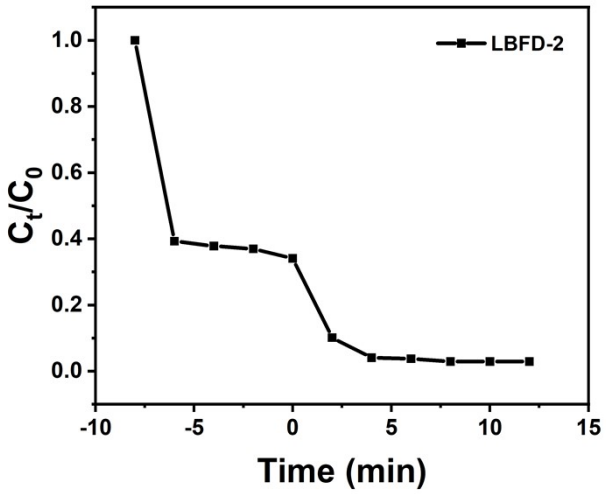

Fig. S13 The removal performance of LBFD-2 towards MB (10 ppm). Dosage of LBFD-2: 0.1 mg mL^{-1}.

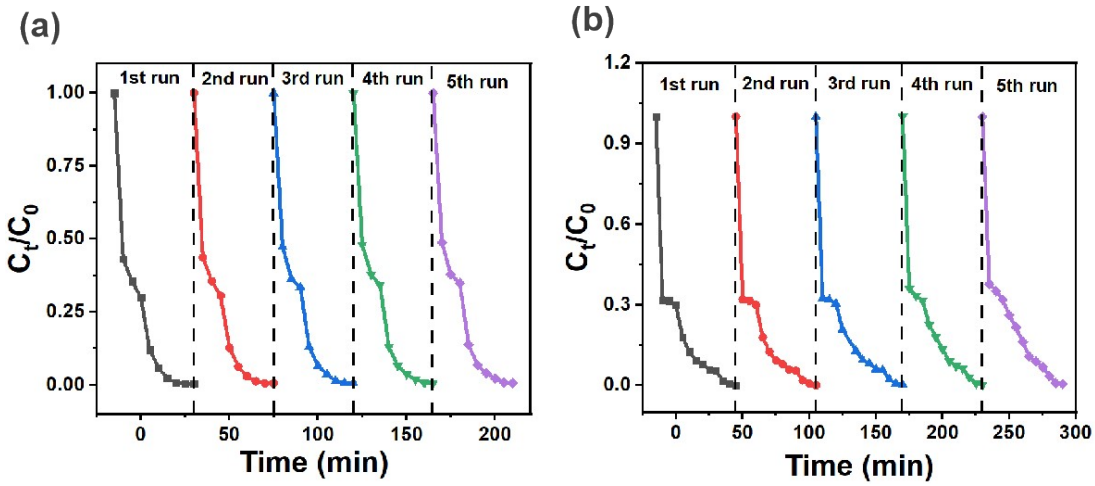

Fig. S14 The reusability of LBFD-2 towards (a) MB and (b) RhB in five cycles.

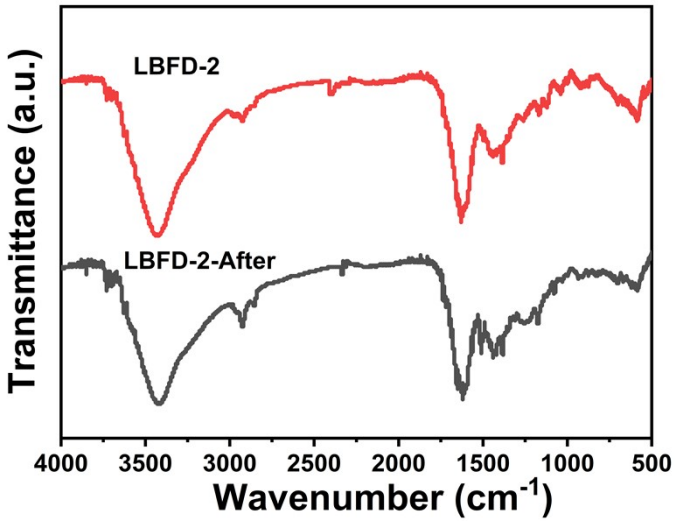

Fig. S15 The FT-IR spectrum of LBFD-2 before and after the degradation process.

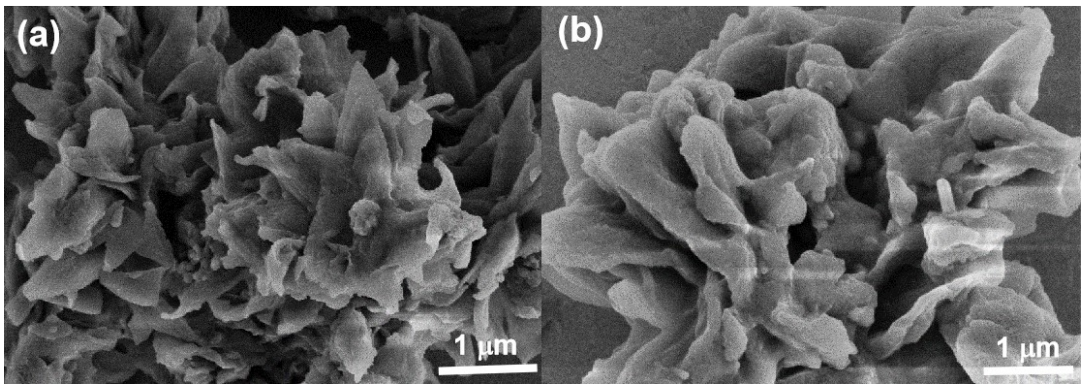

Fig. S16 The SEM images of LBFD-2 (a) before and (b) after the degradation process.

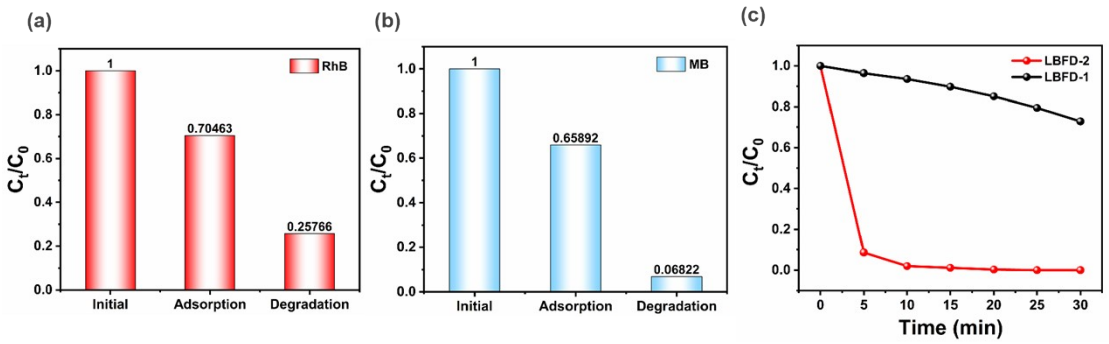

Fig. S17 The percentage of (a) RhB and (b) MB residues in LBFD-2 after dark adsorption and photocatalytic degradation; (c) the removal performance of LBFD-1 and LBFD-2 towards MB (200 ppm) directly under visible light irradiation.

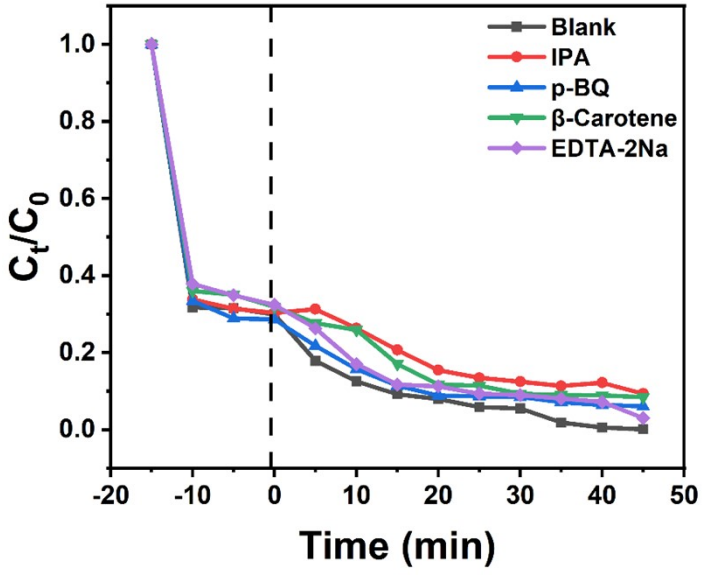

Fig. S18 The photocatalytic degradation performance of LBFD-2 towards RhB with the addition of various quenchers.

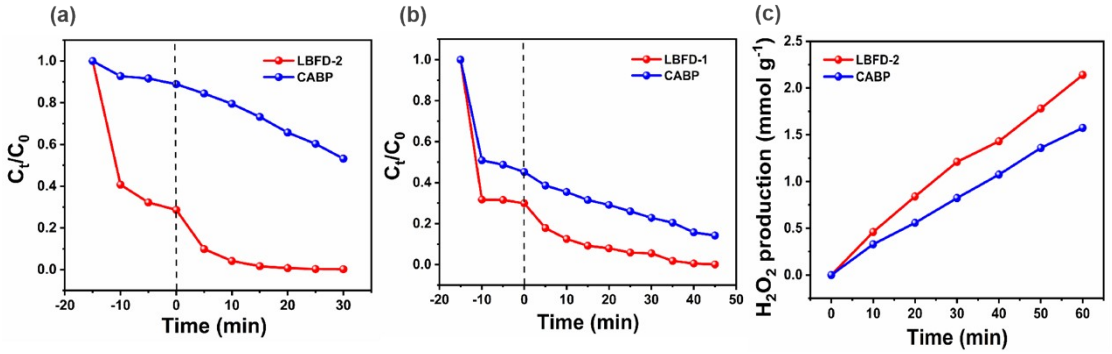

Fig. S19 The degradation performance of LBFD-2 and CABP towards (a) 200 ppm of MB and (b) 50 ppm of RhB, photocatalyst dosage: 0.5 mg mL^{-1}; (c) photocatalytic H_2O_2 production of LBFD-2 and CABP in air.

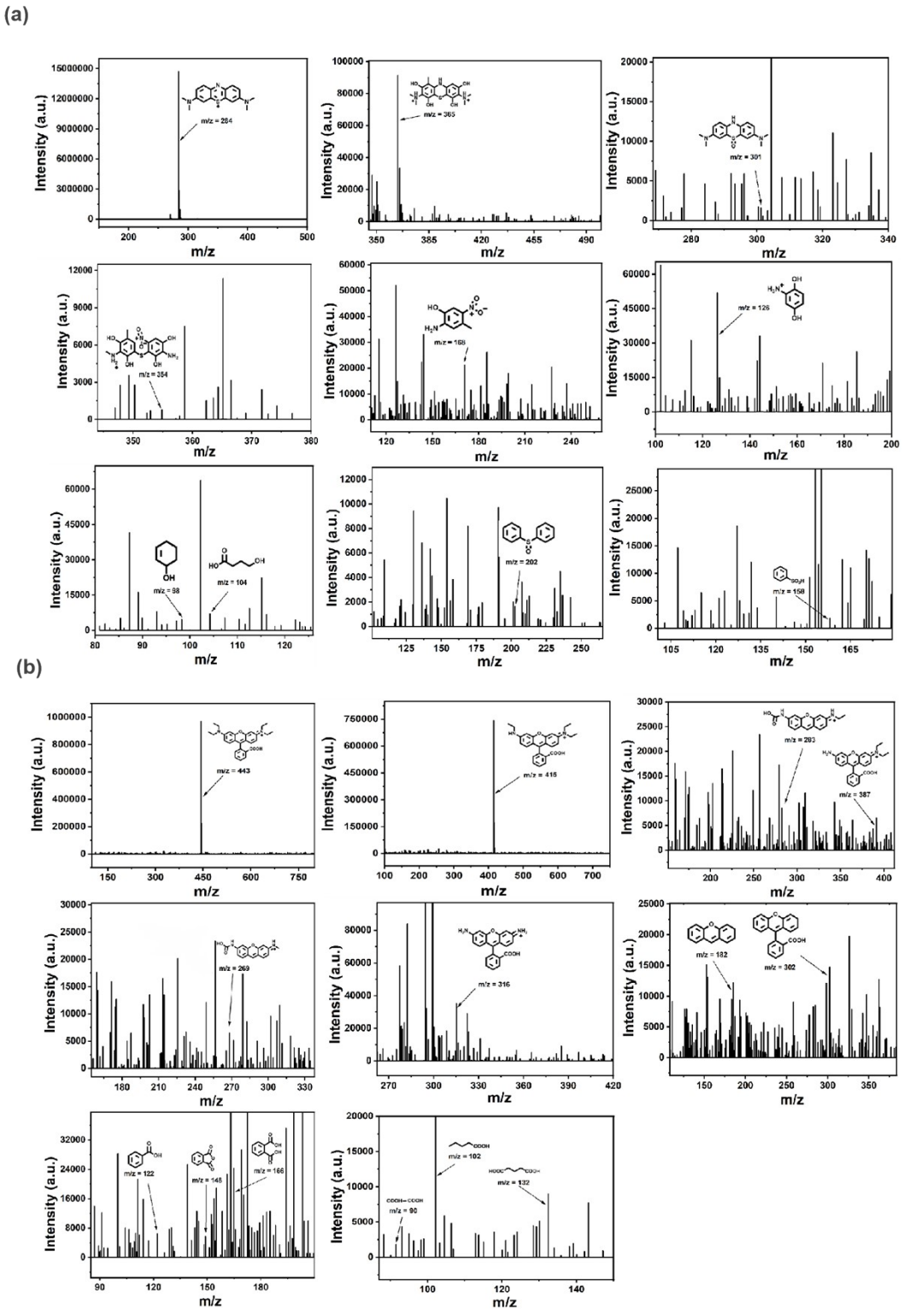

Fig. S20 The LC-MS results of the degradation pathways of (a) MB and (b) RhB.

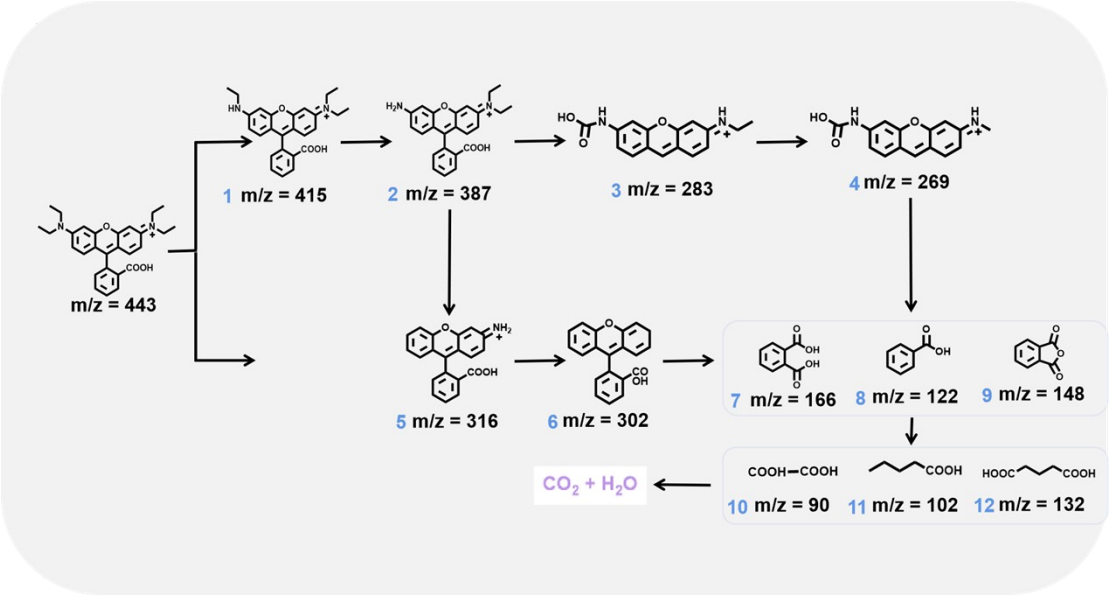

Fig. S21 The potential photodegradation pathways of LBFD-2 towards RhB.

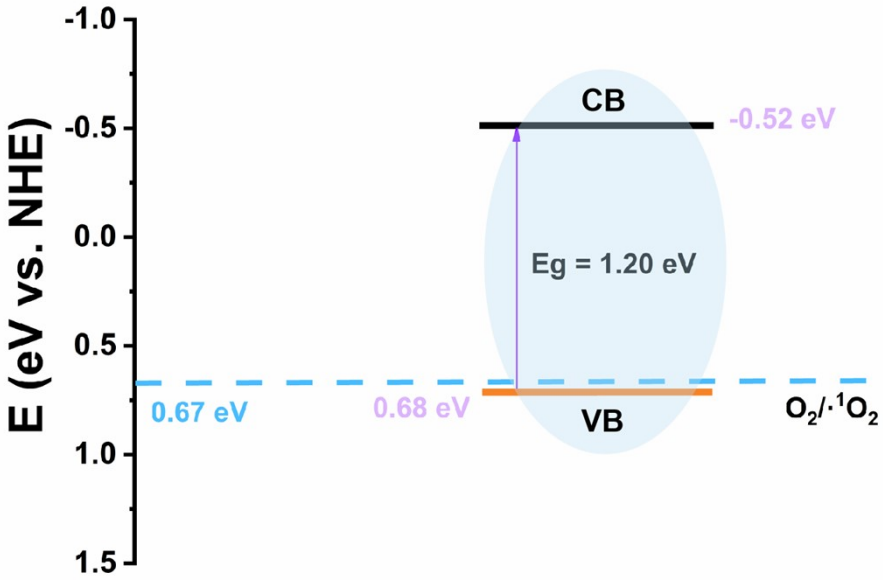

Fig. S22 The potential photodegradation mechanism of LBFD-2 towards MB and RhB under visible light irradiation.

Table S1 Comparison of removal efficiencies of MB by different photocatalysts.

Photocatalyst	Catalyst dosage (g L^{-1})	MB (ppm)	Degradation Time (min)	Reference
g-C_3N_4	1	20	90	[9]
ZrO_2	0.1	10	30	[10]
CABP	0.5	50	20	[11]
TPMnA-COF	0.1	50	660	[12]
CuPT-CPP	0.25	20	120	[13]
LBFD-2	0.5	200	20	This work

Table S2 Comparison of removal efficiencies of RhB by different photocatalysts.

Photocatalyst	Catalyst dosage (g L^{-1})	RhB (ppm)	Degradation Time (min)	Reference
ZrO_2	0.1	10	60	[10]
TMP-P	0.2	20	90	[14]
CuPT-CPP	0.25	20	180	[13]
BOB-CTAB	0.2	10	10	[15]
CQDs-TiO_2	1	10	120	[16]
LBFD-2	0.5	200	40	This work

References

1. D. Wang, R. Malmberg, I. Pernik, S. K. K. Prasad, M. Roemer, K. Venkatesan, T. W. Schmidt, S. T. Keaveney and B. A. Messerle, *Chem. Sci*. 2020, 11, 6256-6267.
2. J. Wang, Y. Lu, N. McGoldrick, C. Zhang, W. Yang, J. Zhao and S. M. Draper, *J. Mater. Chem*. C, 2016, 4, 6131-6139.

3. L. Tian, S. Zhou, J. Zhao, Q. Xu, N. Li, D. Chen, H. Li, J. He and J. Lu, *J. Hazard. Mater*. 2023, 441, 129873.
4. R. Ji, Y. Dong, X. Sun, C. Pan, Y. Yang, H. Zhao and Y. Zhu, *Appl. Catal. B-Environ. Energy*, 2024, 349, 123884.
5. Z. Xu, J. Wang, J. Qiu, H. Cao and Y. Xie, *Environ. Sci. Technol*. 2023, 57, 14442-14451.
6. J. H. Jordan, C. L. D. Gibb, A. Wishard, T. Pham and B. C. Gibb, *J. Am. Chem. Soc.* 2018, 140, 4092-4099.
7. S. Chen, L. Ma, Y. Du, W. Zhan, T. C. Zhang and D. Du, *Sep. Purif. Technol.* 2021, 256, 117788.
8. T. E, X. Xiao and S. Yang, *Sep. Purif. Technol.* 2021, 258, 118070.
9. X. Wang, D. Li and Z. Nan, *Sep. Purif. Technol.* 2019, 224, 152-162.
10. A. H. Kianfar, M. A. Arayesh and M. M. Momeni, *Appl. Phys. A*, 2021, 127, 158.
11. X. Wang, W. Zhao, S. Zhou, G. Liu, D. Wang, X. Li and P. Gu, ACS Appl. Nano Mater. 2024, 7, 7465-7473.
12. S. Rani, N. AlMasoud, S. Rauf, M. A. Khan, M. M. Ahmad, M. Tariq, H. Muhammad Asif and T. S. Alomar, *Tetrahedron*, 2023, 148, 133690.
13. Z. Xu, W. Dong, X. Cui and Q. Duan, *Chemosphere*, 2024, 355, 141801.
14. R. Hu, M. Hassan, L. Liu, S. Zhang and W. Gong, *Chinese Chem. Lett.* 2023, 34, 107541.
15. J. Zhao, T. Guo, H. Wang, M. Yan and Y. Qi, *J. Alloy. Compd*. 2023, 947, 169613.
16. S. Tong, J. Zhou, L. Ding, C. Zhou, Y. Liu, S. Li, J. Meng, S. Zhu, S. Chatterjee and F. Liang, *Colloid. Surface. A*. 2022, 648, 129342.